Jonathan McGlumphy[1]
e-mail: jmcglump@vt.edu

Wing-Fai Ng
e-mail: wng@vt.edu

Department of Mechanical Engineering,
Virginia Polytechnic Institute and State University,
Blacksburg, VA 24061

Steven R. Wellborn
Head of Aerothermal Methods
Rolls-Royce plc,
Derby, England DE73 5AH
e-mail: steven.wellborn@rolls-royce.com

Severin Kempf
Compressor and Fan Aerodynamic Design,
Rolls-Royce Corp.,
Indianapolis, IN 46206
e-mail: severin.g.kempf@rolls-royce.com

3D Numerical Investigation of Tandem Airfoils for a Core Compressor Rotor

The tandem airfoil has potential to do more work as a compressor blade than a single airfoil without incurring higher losses. The goal of this work is to evaluate the fluid mechanics of a tandem rotor in the rear stages of a core compressor. As such, the results are constrained to shock-free fully turbulent flow with thick endwall boundary layers at the inlet. A high hub-to-tip ratio 3D blade geometry was developed based on the best-case tandem airfoil configuration from a previous 2D study. The 3D tandem rotor was simulated in isolation, in order to scrutinize the fluid mechanisms of the rotor, which had not been previously well documented. A geometrically similar single blade rotor was also simulated under the same conditions for a baseline comparison. The tandem rotor was found to outperform its single blade counterpart by attaining a higher work coefficient, polytropic efficiency, and numerical stall margin. An examination of the tandem rotor fluid mechanics revealed that the forward blade acts in a similar manner to a conventional rotor. The aft blade is strongly dependent on the flow it receives from the forward blade, and tends to be more three-dimensional and nonuniform than the forward blade. [DOI: 10.1115/1.3149283]

Keywords: gas turbine, tandem blade, compressor, rotor, computational

1 Introduction

A major limitation on the pressure rise in a subsonic axial-flow compressor stage is boundary layer separation on the blade suction surface and endwalls. One method of mitigating the suction surface separation is to employ tandem airfoil blades (henceforth referred to simply as tandem blades). A 2D profile view of tandem blades is shown in Fig. 1 with their main design parameters. The basic concept is that a new boundary layer forms on the second (aft) blade, allowing for greater overall loading without large flow separations. Tandem airfoils are used as flaps and slats on aircraft to improve lift during takeoff and landing. In turbomachinery, tandem blades have been employed as stators, examples of which include the GE J-79 compressor [1] and an advanced single-stage LP compressor built by Honeywell [2]. However, to the best of our knowledge they have not been used in commercial rotors. This lack of commercial use is the motivation for the current study.

Section 2 of this paper discusses experimental tandem rotors that have been constructed and tested. While the particular machines varied in size and scope, they all shared the shortcoming of narrow stability range from design conditions, which may explain why tandem blades have not yet been employed in commercial rotors.

The goal of this project is to evaluate the fluid mechanics of a tandem blade rotor as applied to the rear stages of a core compressor. That section of the compressor is characterized by high hub-to-tip ratios and fully subsonic shock-free flow at design conditions, a combination that has not previously been examined. If successful, the tandem rotor could be used when high loading is required while maintaining an acceptable overall efficiency and stability margin. It must be noted here that unlike previously tested tandem rotors, this study limits inlet Mach numbers to 0.6 to avoid the complexities of passage shocks.

The first portion of our work examined tandem airfoils numerically in the 2D rectilinear cascade frame of reference. The initial focus on the rectilinear cascade provided insight as to the best arrangement of tandem airfoils to achieve high loading while avoiding excessive profile losses [3].

This paper represents the latter portion of our efforts, which is a viscous numerical study of an isolated tandem rotor in the 3D rotating frame of reference. It should be emphasized that this is a proof-of-concept study, constructed to simulate and understand the differences between 2D and 3D fluid mechanisms of tandem airfoils. Therefore, the tandem rotor presented here represents a simple "first-pass" design. Future work will involve optimizing the blade profiles and three-dimensional stack in addition to addressing mechanical constraints.

2 Literature Review

There is a large body of computational and experimental data on tandem airfoils in 2D cascade available in the open literature. Flow conditions range from incompressible to supersonic. Since our focus is on rear stages of core compressors, we are most interested in the data that is limited to subsonic flow and an axial-velocity density ratio (AVDR) of ~1.0. In Ref. [3] those particular data sets were reviewed and compiled onto a loss versus loading correlation. The Lieblein diffusion factor (henceforth referred to as the D-factor) was used as a measure of airfoil loading, defined here for a 2D tandem airfoil in the cascade frame of reference as

$$D \equiv \left(1 - \frac{w_{22}}{w_{11}}\right) + \left(\frac{w_{\theta,11} - w_{\theta,22}}{2\sigma_{\text{eff}} w_{11}}\right) \tag{1}$$

where the first and second terms represent velocity diffusion and turning, respectively. The associated loss parameter represents the boundary layer momentum thickness at the trailing edge, defined for a 2D tandem airfoil by Eq. (2)

$$\omega_P \equiv \left(\frac{\theta^*}{C_{\text{eff}}}\right) \approx \omega_C \frac{\cos\beta_{22}}{2\sigma_{\text{eff}}}\left(\frac{\cos\beta_{22}}{\cos\beta_{11}}\right)^2 \tag{2}$$

The term ω_C in Eq. (2) is the mass-averaged stagnation pressure loss coefficient, also in the cascade frame of reference

[1]Present address: Synchrony, Inc., 4655 Technology Drive, Salem, VA 24153.

Contributed by the International Gas Turbine Institute of ASME for publication in the JOURNAL OF TURBOMACHINERY. Manuscript received September 29, 2008; final manuscript received January 28, 2009; published March 25, 2010. Review conducted by: David Wisler. Paper presented at the ASME Turbo Expo 2008: Land, Sea and Air (GT2008), Berlin, Germany, June 9–13, 2008.

Downloaded 28 May 2010 to 128.113.26.88. Redistribution subject to ASME license or copyright; see http://www.asme.org/terms/Terms_Use.cfm

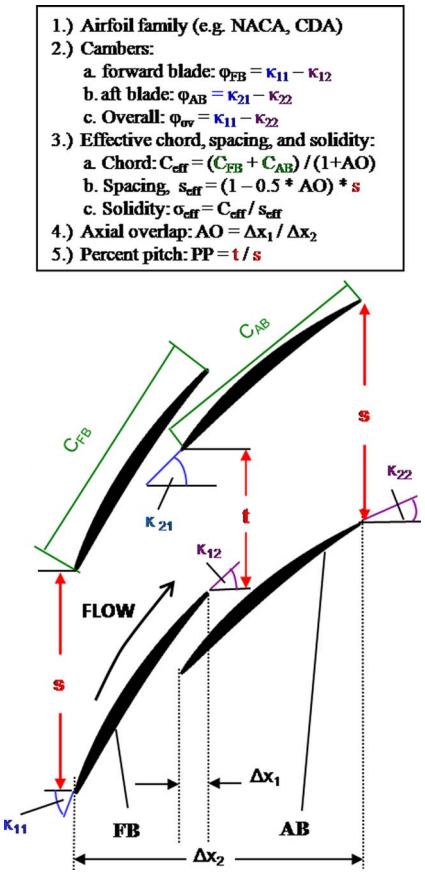

Fig. 1 Tandem blade geometrical parameters

$$\omega_C \equiv \frac{P_{0,11} - P_{0,22}}{P_{0,11} - P_{11}} \tag{3}$$

Large scatter in the pertinent tandem airfoil literature data [3] gave motivation to conduct an extensive 2D computational fluid dynamics (CFD) study evaluating the overall performance as a function of the relative positions of the forward and aft airfoils. The results of that CFD study confirmed that a high percent pitch low axial overlap configuration minimized aerodynamic losses over a wide D-factor range. Figure 2 is a Lieblein loss parameter versus D-factor chart taken from Ref. [3]. It summarizes the results for the "best" tandem airfoil configuration compared with a single airfoil, namely, that a low overlap high percent pitch configuration will achieve lower losses than a comparable single airfoil at a given loading level. The 2D CFD data in Ref. [3] also indicated that a tandem configuration in subsonic flow would have a wider incidence range than a comparable single airfoil.

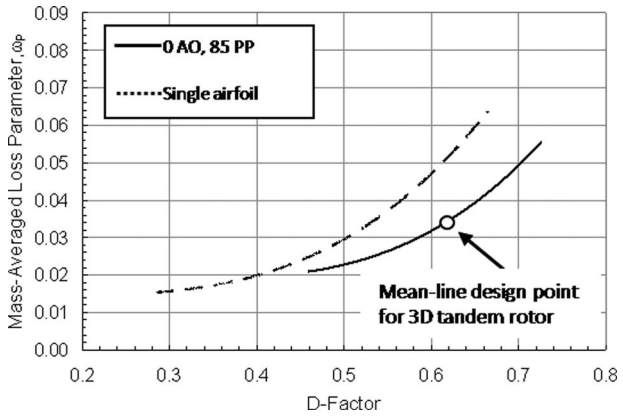

Fig. 2 2D CFD results of single and best-case tandem airfoil from Ref. [3]

Table 1 Design characteristics of previously tested high-speed experimental tandem rotors

Reference	Compressor type	Hub-to-tip ratio ζ	Inlet tip Mach No.
Brent and Clemmons [8]	Single-stage	0.80	0.80
Bammert et al. [9–11]	Multi-stage	0.64	0.85
Hasegawa et al. [12]	Single-stage	Not reported	1.40

3D experimental tandem-type rotors have been in existence since the Second World War. The earliest known example is a slotted-blade low-speed blower tested at the Stuttgart Institute [4]. The reader should distinguish between slotted blades and tandem blades. Slotted blades are created by cutting a gap in a long-chord single airfoil, whereas tandem blades are two distinct airfoils. The Stuttgart data indicated that the slotted-blade blower produced a higher pressure rise but lower efficiency than a comparable single blade blower.

Sheets [5] demonstrated that a well-designed slotted blade blower can achieve both high pressure rise and high efficiency. Linemann [6] conducted a comprehensive series of low-speed tests using a blower with both a tandem rotor and tandem stator. He methodically varied the relative positions of the tandem blades in order to determine the optimum configuration. He concluded that zero axial overlap and 80% pitch produced the greatest pressure rise and efficiency for both the rotor and stator. He also observed that centrifugal effects of the boundary layer had no noticeable effect on the optimum overlap or percent pitch. Railly and Mehra [7] tested a low-speed tandem blade blower. Their traverse data indicated that the highest losses were near the hub, but they were unable to provide details of the 3D fluid mechanisms.

Of greater relevance to the current study are the higher-speed tandem rotors of Refs. [8–12]. The major design characteristics of these machines are shown in Table 1.

Brent and Clemmons [8] compared a single-blade rotor to two different tandem rotors. All three rotors were designed for a work coefficient of 0.50 and polytropic efficiency of 91.2%. The two tandem rotors differed in loading split between the forward and aft blades: one had a 50/50 split and the other had a 20/80 split. The 50/50 split rotor achieved pressure ratio only 4.5% below the design value and met the design efficiency. Both the 20/80 tandem and the single-blade rotor fell considerably short of the design criteria. Both of Brent and Clemmons' tandem rotors had a surge margin of 17%, defined by Eq. (4) [13], which were approximately the same as the single-blade rotor

$$SM = 1 - \left\{ \left(\frac{PR_{\text{design}}}{PR_{\text{surge}}} \right) * \left(\frac{\dot{m}_{\text{surge}}}{\dot{m}_{\text{design}}} \right) \right\} \tag{4}$$

Bammert et al. [9–11] tested a multistage compressor that consisted of a single-blade rotor, three tandem rotors, and another single-blade rotor (front to back). All stators were single-blade. At nominal flow the compressor developed an average overall (i.e., whole machine) work coefficient of 0.77 and a polytropic efficiency of 85.6%. The surge margin from nominal was less than 5%. It is also noteworthy that Bammert's compressor reached peak efficiency at 70% of design speed. This was attributed to "the decreasing influence of the Mach number." Traverse data between the stages indicated that the highest losses were near the hub.

Hasegawa et al. [12] tested a single-stage transonic tandem blade compressor. At nominal flow the stage developed a work coefficient of 0.51 and a polytropic efficiency of 79.4%. Surge

Downloaded 28 May 2010 to 128.113.26.88. Redistribution subject to ASME license or copyright; see http://www.asme.org/terms/Terms_Use.cfm

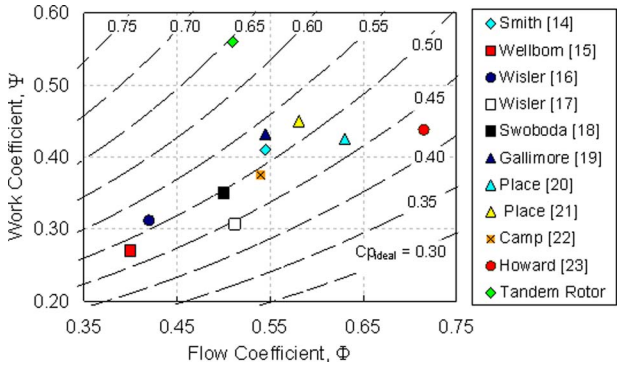

Fig. 3 Selected single blade compressor and tandem rotor design points

margin was approximately 10%, while there was very little choke margin. Traverse data indicated that losses were higher at the tip than at the hub. While the transonic tandem rotor had been analyzed with a fully 3D viscous flow solver, the effects of tip clearance were not considered.

This study examines the tandem rotor in a very specific application: the rear stages of core compressors. It is hypothesized that a tandem rotor may prove to be a worthwhile alternative to conventional stages in that part of an engine.

3 Method of Analysis

As already mentioned, the purpose of this paper is to extend the earlier 2D cascade tandem airfoil work into the 3D rotating frame of reference. One of the objectives of the 3D CFD study is to evaluate the overall performance of a first-pass tandem rotor design and compare it to a geometrically similar single-blade rotor.

The second—and more important—objective is to evaluate the 3D fluid mechanisms present in a tandem rotor. Experimental research on tandem rotors [8–12] has provided limited insight into the 3D flows, mainly via downstream traverse data. CFD simulations allow for more a detailed analysis of the flow field than has been previously published.

Stators are not considered in this study. However, given the high level of swirl that could be present at the exit of a tandem rotor, a well-designed stator will be essential to the performance of a whole stage. The knowledge gained from the tandem rotor flow field should prove useful in the future task of designing a robust stator for use in a tandem rotor/single stator stage.

3.1 Tandem Rotor Constraints and Design Goal. The mean-line design goal for the tandem rotor was chosen to match the profile losses of a single airfoil near $D=0.50$. This corresponded to a D-factor of ~0.62 of the best tandem airfoil in the 2D study (Fig. 2). Based on the flow angles from the 2D study, the isolated tandem rotor geometry was targeted to produce a work coefficient, ψ, of 0.56 at a flow coefficient, Φ, of 0.51. This goal represents the potential duty of a 2D tandem blade geometry assuming no 3D flow, shown on the Smith chart in Fig. 3 along with values from several conventional rear stage configurations from open literature [14–23]. As can be seen, the tandem rotor target is above published levels by over 50%. However, the reader should bear in mind that only a rotor is being considered here, whereas the literature data are for complete stages.

To avoid the complexities of passage shocks the previous 2D study was limited to subsonic flow, typical in the rear stages of a core compressor. This design constraint was maintained in the 3D analysis. The design tip speed was 698 ft/s, resulting in an inlet relative tip Mach number of 0.62 with a relative inlet flow angle, β_{11}, of 62.0.

All of the tandem configurations in Ref. [3] were designed such that the forward and aft airfoils had a 50/50 loading split, i.e., equal individual D-factors. This was partially based on Brent and Clemmons' [8] report that a 50/50 split performed better than a 20/80. It was also observed in the 2D literature that uneven loading splits tended to produce higher losses than equal loading splits. This trend was verified by McGlumphy [24] in a separate 2D CFD study and was maintained for this 3D rotor design.

3.2 Tandem Rotor Geometry. The 2D tandem geometry meeting the design goals and constraints was simply extruded to a 3D blade intended for use in the high reaction rear stage of a core compressor. The blade was not altered to accept incoming flow at the endwalls, having constant geometric parameters across the span. In addition, a high hub-to-tip ratio ($\zeta > 0.95$) and a low aspect ratio were imposed. See Table 2 for the detailed geometric parameters.

The 2D perturbation study in Ref. [3] used a simple tandem airfoil design rule to generate the geometries for a wide range of overall D-factors. This design rule necessitated an extensive knowledge of the chosen airfoil family in order to provide accurate estimates of the required metal angles and cambers of the forward and aft airfoils. While not the most potent of airfoils, there is a large amount of openly available data on the NACA-65 family [25], which made it a convenient choice for use in the simple design rule. In order to keep the 2D tandem design rule from being overly complex, all tandem configurations had equal forward and aft airfoil chords. Blade loadings were varied by altering only cambers and stagger angles.

3.3 Single Blade Rotor Geometry. A single blade configuration was generated as a baseline case to emphasize that the design point chosen for the tandem blade is well out of the normal design space for single airfoils. This single blade was the same airfoil family and had the same overall camber, effective chord and solidity, thickness (as a percentage of blade chord), and thickness distribution as the blades for the tandem rotor. Their respective 2D profiles are shown in Fig. 4. The single blade rotor was subject to the same boundary conditions and near wall meshing constraints as the tandem blade rotor.

3.4 CFD Setup and Procedure. The tandem rotor mesh configuration was developed using a standard H-mesh for both the forward and aft blades. The domain was split into four regions: a lower passage, an upper passage, inlet block, and exit block, as shown in Fig. 5. Connectivity was maintained at the boundaries of each region using a direct patch boundary condition—computational lines in the i, j, and k directions are 1:1 across the boundary. Near-wall spacing was set on the blade surfaces in the tangential direction, and points were clustered axially at the leading and trailing edges of each blade. The tangential spacing tran-

Table 2 Current tandem rotor geometric parameters

	Chord (in.)			Camber (deg)						Tip clearance (both blades)	
Airfoil family	Forward blade	Aft blade	Effective	Forward blade	Aft blade	Overall	σ_{eff}	AO	PP	% span	% effective chord
NACA-65	0.6675	0.6675	1.335	20.1	39.3	48.0	1.93	0.0	85.0	1.1	0.5

Downloaded 28 May 2010 to 128.113.26.88. Redistribution subject to ASME license or copyright; see http://www.asme.org/terms/Terms_Use.cfm

Fig. 4 Tandem (L) and single rotor (R) 2D profiles

sitioned to equal cell spacing at the inlet and exit of the computational domain. Over 1.1×10^6 grid points were used to discretize the domain. Stators were not included in any of the simulations.

The CFD solver employed is called advanced ducted propfan analysis code (ADPAC), a Reynolds-averaged Navier–Stokes (RANS) code that was developed specifically to analyze ducted turbofan engines. Time-marching was carried out by the explicit, four-stage Runge–Kutta scheme. ADPAC has three available turbulence models: Baldwin–Lomax algebraic, Spalart–Allmaras one-equation, and Goldberg two-equation. Detailed descriptions of each are given in Ref. [26]. The Baldwin–Lomax turbulence model with wall functions was used in this study. Solutions typically converged within 500 iterations; 800 iterations was the maximum.

The flow was assumed to be periodic in the pitchwise direction. Endwalls and blades (excluding the tip clearance region) were modeled as solid viscous surfaces with no-slip imposed. Tip leakage flow was modeled using a periodic boundary condition between the respective blade pressure and suction sides of the gap. A final consideration was that by the rear stages of a core compressor, the hub and casing boundary layers have usually developed to a significant thickness. In order to model this, a defect in stagnation pressure was imposed at the inlet to the tandem and single blade rotors. This defect extended outwards by 30% blade span from both endwalls, and is shown in Fig. 6 as a percentage of the freestream stagnation pressure in the core flow region. Blockage due to this defect was approximately 6%.

Only 100% rotational speed was considered for both the tandem and single blade rotor. Exit static pressure was varied at constant rotational speed in order to generate a speed-line. The rotors were considered stalled at one of two conditions: mass flow decreased rapidly or large mass flow oscillations occurred.

2D grid independency had been previously verified by increasing the number of axial and pitchwise points until pertinent aerodynamic quantities (e.g., incidence and turning) no longer changed for a given set of boundary conditions [3]. The same procedure was repeated in the radial direction to establish the minimum number of points for grid-independent 3D solutions.

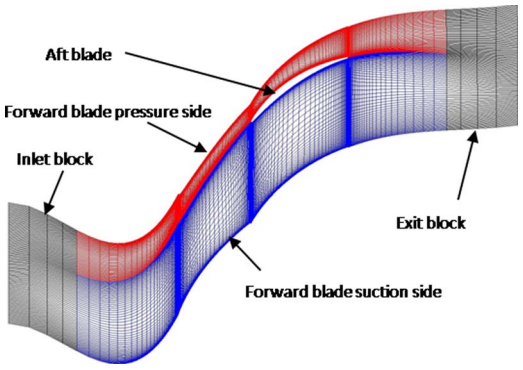

Fig. 5 Tandem rotor CFD mesh (profile view)

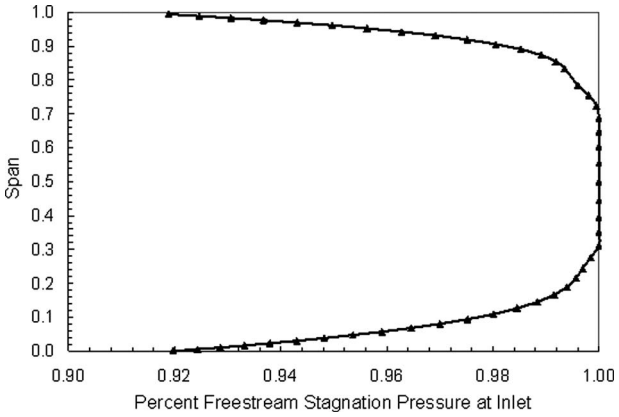

Fig. 6 Tandem rotor inlet total pressure profile

4 Results

The results are presented in two sections. Section 4.1 reviews the tandem rotor overall performance. Sections 4.2–4.4 provide insight into the flow field of a tandem rotor including differences between the forward and aft blades.

4.1 Overall Performance. Figure 7 shows the speed-line characteristics of the tandem and single blade rotors at 100% design speed. Mass-averaged work coefficient and polytropic efficiency (rotor only) are plotted versus flow coefficient, which here is the inlet mean axial velocity across the entire blade span normalized by tip speed. Also included is the single point 3D equivalent value taken from the 2D cascade studies at minimum loss (no 3D flow imposed).

It can be seen from Fig. 7 that the tandem rotor does not meet

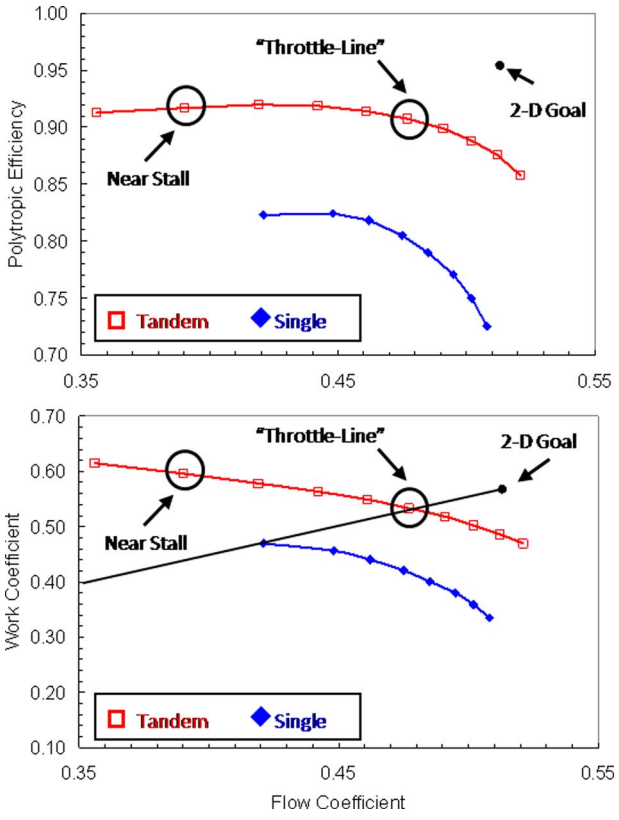

Fig. 7 Tandem and single rotor 100% speed performance characteristics

Downloaded 28 May 2010 to 128.113.26.88. Redistribution subject to ASME license or copyright; see http://www.asme.org/terms/Terms_Use.cfm

the target performance, designated by the equivalent 2D goal. Instead, along an approximate constant throttle line, the 3D rotor produces a work coefficient of 0.53 at a mean flow coefficient of 0.48. The miss in target performance (~5%) obviously comes from the 3D flow field, as opposed to 2D cascade flow, which will be discussed later. The polytropic efficiency at this operating point is 91%, while the peak efficiency is near 92% (corresponding to a work coefficient of 0.56). While not at industry leading efficiency levels, it should be noted the equivalent 2D polytropic efficiency is 96%, suggesting a significant amount of 3D losses that could be mitigated. By comparison, the single rotor only achieves a dismal peak efficiency of 82.4% at $\Phi=0.45$, and at no point does it match the tandem rotor loading. This simply indicates that the geometrically single rotor would not be chosen to operate in such an aggressive design space.

Using Eq. (4), the tandem rotor has a numerical stall margin of approximately 19% from the constant throttle line and 10% from peak efficiency. In reality the tandem rotor stall margin could be even higher than what is seen in Fig. 7, since CFD tools commonly underpredict stall margin.

Conventional rear stage core compressor rotors are not designed with the level of loading achieved in the tandem rotor, owing to the obvious poor performance of the single rotor, as seen in Fig. 7. Neglecting the pressure losses across a stator for the moment, the increased work coefficient of around 50% from conventional designs (Fig. 3) suggests that a realistic estimate of the tandem rotor potential in a core compressor is to replace three conventional stages with two tandem rotor stages. Of course, this is based solely on the aerodynamic loading capability of the tandem rotor. A tandem rotor would necessarily require a wider disk than a convention rotor. However, from a system perspective, the possible engine length savings may provide a greater benefit than the penalty incurred from the thicker tandem rotor disk. In any event, the authors recognize that the tandem rotor cannot be considered superior to a conventional rotor simply by comparing it to the single blade rotor shown in Fig. 4. A full system study will ultimately be necessary to conclusively determine if the tandem rotor is commercially viable.

In order to properly design a whole stage using tandem rotors, three main challenges must be met. The first would be to boost the rotor efficiency levels slightly above the levels seen in Fig. 7 by mitigating 3D flows. The second challenge would be to design a stator that can turn the flow from the tandem rotor without introducing prohibitively high losses. The third, admittedly, is a host of mechanical issues that are beyond the scope of this work.

An understanding of the complex flow mechanisms in a tandem rotor passage will help address the first two challenges. As such, Sec. 4.2–4.4 focuses on the flow field within the tandem rotor.

4.2 Tandem Rotor Fluid Mechanics. The fluid mechanics that is unique to a 2D tandem airfoil is documented in Ref. [3]. There are two relevant phenomena for the particular configuration examined in this paper. The first is that at high percent pitch the aft blade induces additional circulation onto the forward blade. This effect was considered when specifying the camber of the forward blade in order to maintain a 50/50 loading split. The second effect is accelerating flow in the converging gap region formed at the interface of the forward blade trailing edge and the aft blade leading edge.

The 2D and 3D fluid mechanics of a conventional rotor are well documented. Reference [13] is a good example. This portion of the paper highlights the fluid mechanics of a 3D tandem rotor, and in particular the differences between the behavior of the forward and aft blades. Focus is placed on two operating conditions: the "throttle-line" ($\Phi=0.48$) and near stall ($\Phi=0.39$), as shown in Fig. 7. The near stall point represents the condition where the forward blade core region flow best matches the 2D equivalent. The 2D equivalent values from the cascade studies [3] are also provided for comparison.

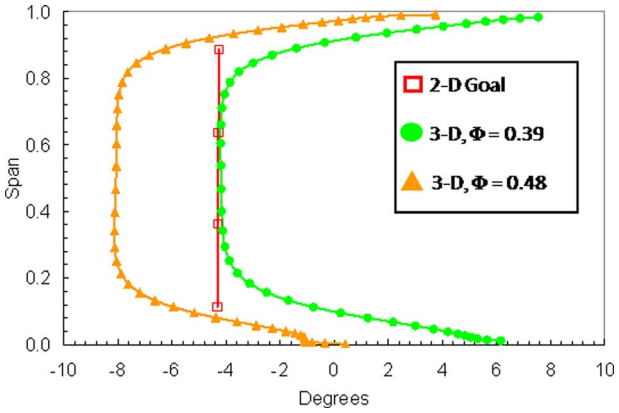

Fig. 8 Forward blade incidence

4.3 Forward Blade Fluid Mechanics. Figures 8–10 represent the forward blade spanwise distributions of incidence, deviation, and total pressure loss coefficient. For losses (Eq. (3)), total pressures were mass-averaged across the pitch at each radial location and normalized by the forward blade inlet values. The values were collected 2% chord upstream and downstream of the forward blade. During discussions of the flow field, the hub region is defined as 0–30% span, the core region as 30–70% span, and the tip region as 70–100% span.

It can be seen in Figs. 8–10 that the forward blade at the near stall condition (circles) nearly matches the 2D values (squares) in the core region with only a small 1 deg difference in core flow deviation. At throttle-line conditions, the forward blade incidence

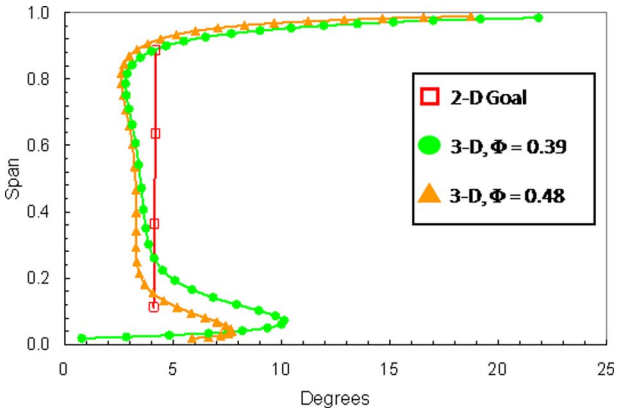

Fig. 9 Forward blade deviation

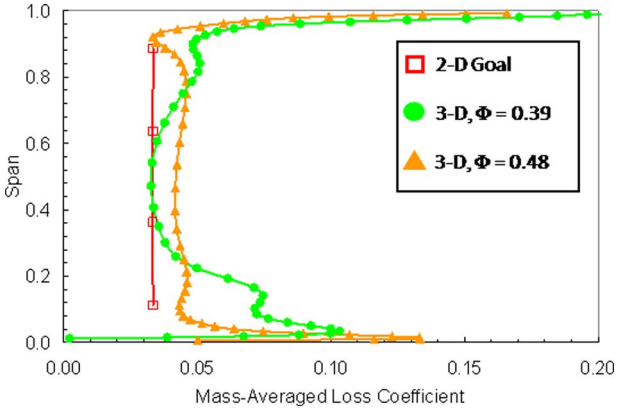

Fig. 10 Forward blade losses

Downloaded 28 May 2010 to 128.113.26.88. Redistribution subject to ASME license or copyright; see http://www.asme.org/terms/Terms_Use.cfm

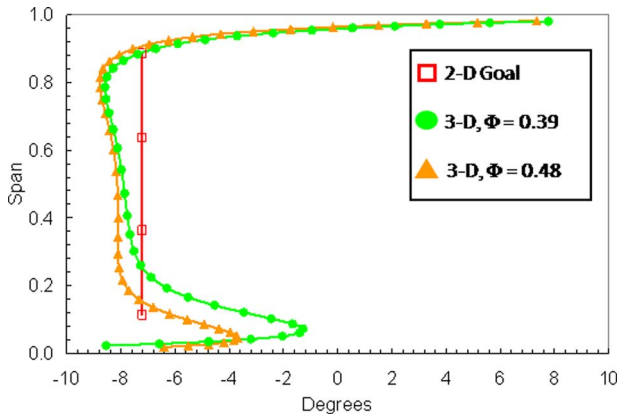

Fig. 11 Aft blade incidence

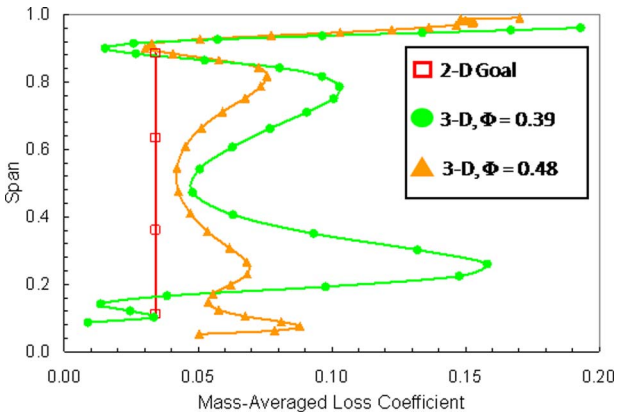

Fig. 13 Aft blade losses

across the entire span is 3–4 deg lower. This difference in incidence does not profoundly affect the forward blade deviation in the core region, but slightly increases losses due operating closer to the negative stall side of the 2D loss bucket. Therefore, the core flow of the forward blade acts similarly to the 2D cascade equivalent.

The flow is skewed at both the hub and tip regions, which is expected given the thick boundary layer at both endwalls, creating more positive incidence values there for the forward blade (Fig. 8). This higher endwall incidence pushes the forward blade well above a 0.6 D-factor at the endwalls, resulting in higher deviation and losses than the 2D cascade values (Figs. 9 and 10). In addition, both the hub and tip develop classical secondary flow features due to the incoming vorticity profile. The hub region features underturned flow near 10% span and overturned flow very near the hub with increased hub region losses due to the secondary flow. The tip region features underturned flow and increased losses due to leakage flow. As expected, with increased endwall incidence and loading (going from throttle-line to near stall conditions), the deviation and loss values increase there. Therefore, although the endwall regions do not act like 2D cascade flow, they are not dissimilar to conventional rotor blade fluid mechanics. This has design implications, since traditional techniques to reduce endwall loss should be applicable to the forward blade.

4.4 Aft Blade Fluid Mechanics. Figures 11–13 represent the aft blade spanwise distributions of incidence, deviation, and total pressure loss coefficient. For aft blade losses (Eq. (3)), total pressures were mass-averaged across the pitch at each radial location and normalized by the aft blade inlet values. The values were collected 2% chord upstream and downstream of the aft blade, meaning that the mixing losses from the forward blade wake are partially manifest in the aft blade 2D and 3D loss profiles.

Since the forward blade discharges the air at a slightly lower deviation value, the incoming incidence values of the aft blade are slightly more negative than the 2D cascade in the core region. This tends to offload the airfoil in the core region, making it operate slightly off minimum loss incidence. In addition the aft blade endwall regions have increased incidence due to the underturning of the fluid of the forward blade, except very near the hub.

Like the forward blade, the deviation of the aft blade is close to the 2D values in the core region. The radial gradient in deviation through the core region is due to overall passage secondary flow as in a conventional rotor. Deviation increases going toward the hub, but then decreases rapidly around 10% span, showing additional overturning of the flow by the aft blade at the hub. The flow also has higher-than-2D deviation near the tip, again due to the tip clearance.

The aft blade loss profiles, however, differ from the forward blade, suggesting that the 3D behavior is more severe than a conventional rotor. This can be seen in Fig. 14, which shows contours of radial components of velocity on the suction surfaces of both blades at the throttle-line operating condition. The forward blade has a region of downward flow (i.e., toward the hub) at the leading edge near the hub, and upward flow near the blade tip. By contrast, the aft blade has a large region of upward radial flow from around 30–90% chord.

The aft blade hub region losses are higher than in the forward blade hub region. This is reasonable since the low-momentum high-entropy flow from the forward blade trailing edge at the end-

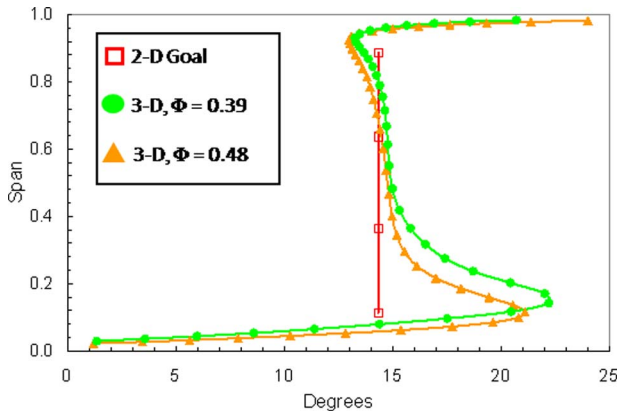

Fig. 12 Aft blade deviation

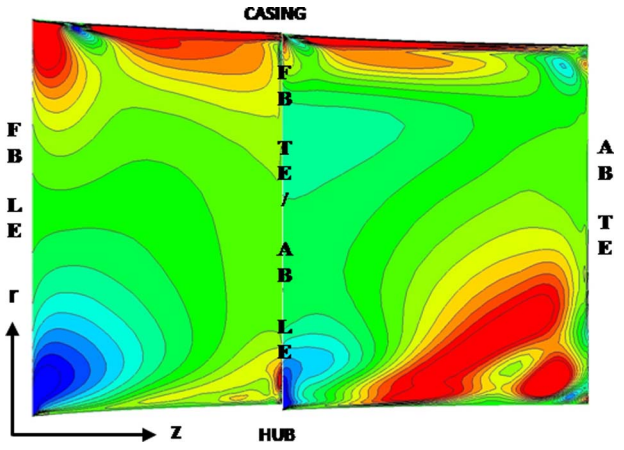

Fig. 14 Suction surface radial velocity contours

Downloaded 28 May 2010 to 128.113.26.88. Redistribution subject to ASME license or copyright; see http://www.asme.org/terms/Terms_Use.cfm

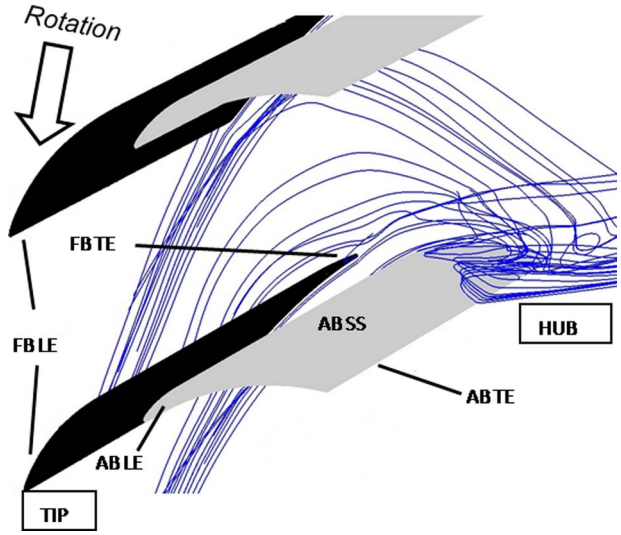

Fig. 15 Tandem rotor flow passage with streamlines seeded near the hub

wall discharges directly on to the aft blade leading edge. Additionally, the overturned high-entropy flow from the forward blade hub is directed toward the aft blade suction side-endwall corner at the trailing edge, visualized in Fig. 15. The result is that hub losses extend further into the core region. It is worth noting that in a conventional rotor the low-momentum hub region flow can be re-energized due to the change in reference to the next blade row. This can be beneficial because it opposes the secondary flow. However, that is not the case here with the forward blade hub flow overturned onto the aft blade, and may limit the tandem rotor's efficiency potential in a multistage environment.

Another difference between the forward and aft blades is flow uniformity. Figures 16 and 17 show entropy contours in the radial-tangential plane at the forward blade/aft blade interface and the aft blade trailing edge, respectively, looking upstream. At both operating conditions shown the aft blade exit flow is more nonuniform than the forward blade exit flow due in part to the wake from the forward blade mixing out into the freestream flow. However, the entropy generated by forward blade wake mixing is less than that at the hub, particularly at $\Phi=0.48$ (Fig. 17(*a*)). The aft blade exit nonuniformities will be a key consideration when designing a stator to handle the incoming flow from the tandem rotor.

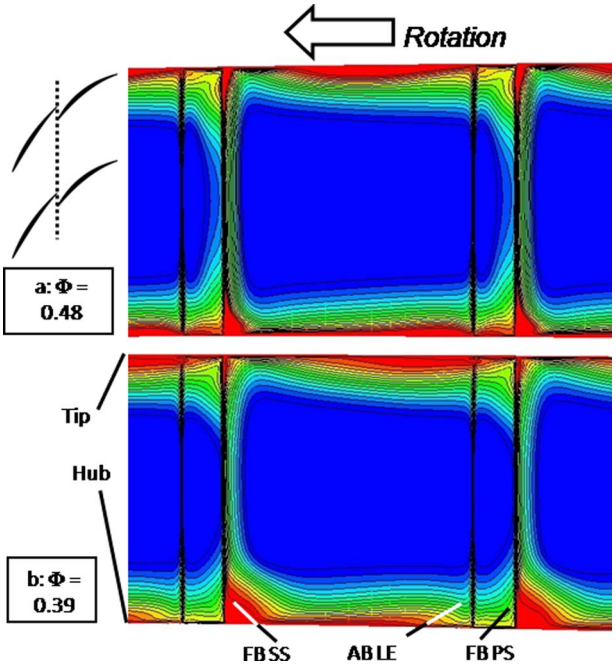

Fig. 16 Entropy contours at forward blade/aft blade interface looking upstream

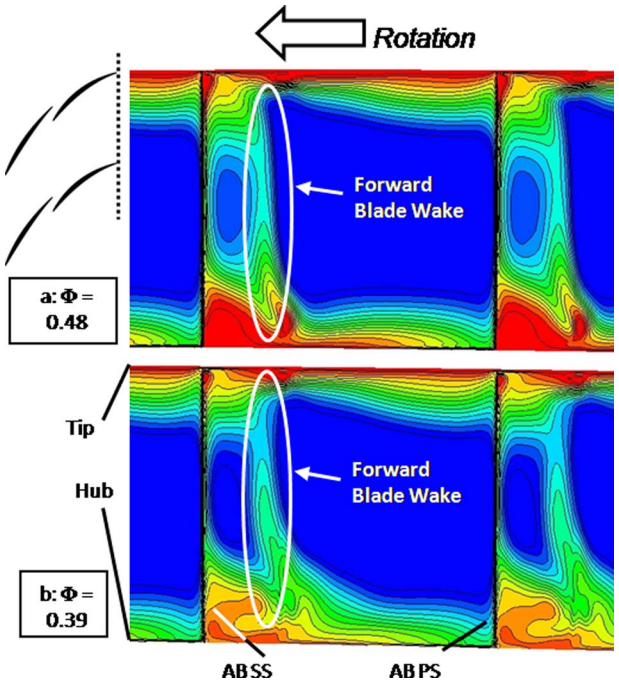

Fig. 17 Entropy contours at aft blade trailing edge looking upstream

A final comment concerns the blade loading split, which had been set to 50/50 based on the previous 2D work. Figure 18 is a plot of blade surface Mach number at 10%, 50%, and 90% span at the peak efficiency operating condition. The aft blade loading differs more from the hub to tip than does the forward blade, which is not surprising given the more 3D nature of the aft blade flow. It may well be that while a 50/50 split is the best design in 2D, in 3D the loading split should vary across the span in order to optimize the whole rotor.

4.5 Summary of Tandem Rotor 3D Flows. The forward blade tends to behave like a conventional rotor across the operating range. Near stall, the forward blade endwall losses are higher

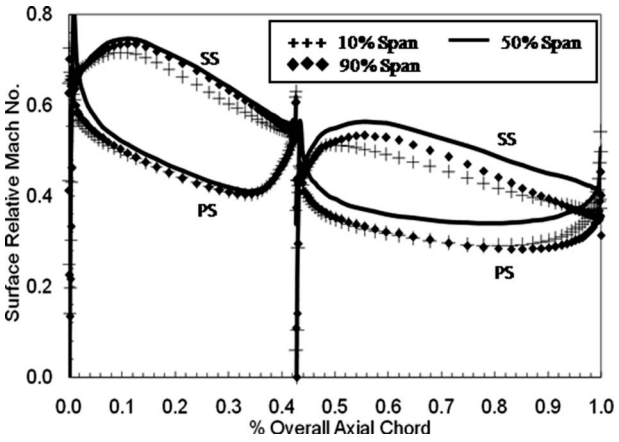

Fig. 18 Blade loading distributions

Downloaded 28 May 2010 to 128.113.26.88. Redistribution subject to ASME license or copyright; see http://www.asme.org/terms/Terms_Use.cfm

than at midspan due to positive incidence in those regions and conventional secondary flow features. The hub region is the most affected due to high local loading coupled with the interaction at the suction side-endwall corner.

The aft blade acts less like a conventional rotor than the forward blade. It is strongly affected by the forward blade exit flow, and has highly 3D flow that differs from what is seen in a conventional rotor. High losses from the forward blade hub region propagate downstream to the aft blade. Additionally, overturning at the hub region of the forward blade directs high-entropy fluid toward the aft blade suction side-endwall corner, resulting in high aft blade hub region loss and flow nonuniformities. Low-energy fluid from the aft blade hub region propagates radially outward toward the core. The aft blade loss distributions are complicated by the mixing of the forward blade wake. The aft blade losses could be reduced if the incoming flow is improved. In hindsight, it seems somewhat intuitive that the aft blade is strongly dependent on the forward blade. The numerical results shown here provide evidence to support that idea.

Recall that Railly and Mehra [7] and Bammert et al. [9–11] reported high losses in the hub region of their experimental rotors, but did not offer a complete explanation for why that was the case. It is entirely possible that they did not foresee the magnitude of the forward blade/aft blade relationship described above, and did not give it full consideration during their design process.

5 Conclusion

The tandem airfoil concept has been revisited to evaluate its potential as a rotor in a very specific application that has not been previously examined: the rear stages of a core axial-flow compressor. It must be emphasized that the conclusions drawn from this study should be considered valid within certain constraints, namely, a high hub-to-tip ratio, subsonic, shock-free, fully turbulent flow, and thick endwall boundary layers at the inlet. Also, given that this is a numerical study, the results shown should be taken as an indication of trends, and not necessarily as absolute performance levels.

A simple geometry was developed based on the best-case tandem airfoil configuration from a previous 2D study. The 3D tandem rotor was simulated without a stator in order to scrutinize the fluid mechanisms of the rotor before pursuing design of a whole stage.

The tandem rotor examined in this paper has sufficient aerodynamic loading capability to replace three conventional core compressor rotors with two tandem rotors. Efficiency was below industry standards, although that could be mitigated by improving the design, i.e., accounting for spanwise variation in the flow during the design process.

The CFD solutions indicated that the forward blade behaved in a similar manner to a conventional rotor, whereas the aft blade did not. High-entropy low-momentum fluid from the forward blade had an adverse effect on the aft blade. The aft blade flow was highly nonuniform compared with the forward blade. Reducing the forward blade losses should have a noticeably favorable effect on the aft blade.

Aknowledgment

The authors express their thanks to Rolls-Royce Corporation for providing financial support for this project and for permission to publish the results. We also are grateful to Mike Howard for helping collect the Smith chart data.

Nomenclature

AB = aft blade
AO = axial overlap of tandem blades
AVDR = axial-velocity density ratio
C = chord
D = Lieblein diffusion factor
FB = forward blade
LE = leading edge
$\dot{m}$ = corrected mass flow
P = pressure
PP = percent pitch of AB LE relative to spacing
PS = pressure side
PR = pressure ratio
SM = surge margin
SS = suction side
r = radial coordinate
TE = trailing edge
t = pitchwise spacing between FB TE and AB LE
w = velocity in cascade frame of reference
z = axial coordinate

Subscripts

eff = effective
0 = stagnation conditions
11 = forward blade inlet station
12 = forward blade exit station
21 = aft blade inlet station
22 = aft blade exit station

Greek

β = flow angle relative to axial coordinate
Δx_1 = axial distance between FB TE and AB LE
Δx_2 = axial distance between AB TE and FB LE
ψ = work coefficient, $\Delta h_0 / U^2_{\text{tip}}$
ζ = hub-to-tip radius ratio
θ = pitchwise coordinate
θ^* = boundary layer momentum thickness at TE
κ = airfoil metal angle relative to axial coordinate
σ = solidity, C/s
φ = camber
Φ = flow coefficient, V_z/U
ω_C = stagnation pressure loss coefficient
ω_P = momentum thickness loss parameter

References

[1] Gostelow, J. P., 1984, *Cascade Aerodynamics*, Pergamon, New York, Chap. 9.
[2] Barton, M. T., and Gentile, D. P., 2005, "The Use of a Circumferentially Nonuniform Stator to Attenuate Harmful Aerodynamic and Mechanical Interactions in an Advanced Mixed Flow Splittered Rotor/Tandem Variable Stator LP Compressor," ASME Paper No. GT2005-68178.
[3] McGlumphy, J., Ng, W., Wellborn, S., and Kempf, S., 2007, "Numerical Investigation of Tandem Airfoils for Subsonic Axial-Flow Compressor Blades," ASME Paper No. IMECE2007-43929.
[4] Schroeder, W. M., 1945, "Axial Flow Compressor Development at the Stuttgart Research Institute," H. M. Stationery Office, CIOS Item No. 19, File No. XXXII-31.
[5] Sheets, H. E., 1955, "The Slotted-Blade Axial-Flow Blower," ASME Paper No. 55-A-156.
[6] Linnemann, H., 1964, "Untersuchungen Eines Einstufigen Axialgelblases mit Tandemgittern," Konstruuktion, Heft 4, S 128.
[7] Railly, J. W., and Mehra, S. M., 1969, "Experimental Investigation of Tandem Axial Compressors," Proc. Inst. Mech. Eng., **184**(2), pp. 9–16.
[8] Brent, J. A., and Clemmons, D. R., 1974, "Single-Stage Experimental Evaluation of Tandem-Airfoil Rotor and Stator Blading for Compressors," NASA Report No. CR-134713.
[9] Bammert, K., and Staude, R., 1979, "Optimization for Rotor Blades of Tandem Design for Axial Flow Compressors," ASME Paper No. 79-GT-125.
[10] Bammert, K., and Beelte, H., 1980, "Investigations of an Axial Flow Compressor With Tandem Cascades," ASME J. Eng. Power, **102**, pp. 971–977.
[11] Bammert, K., and Staude, R., 1981, "New Features in the Design of Axial-Flow Compressors With Tandem Blades," ASME Paper No. 81-GT-113.
[12] Hasegawa, H., Matsuoka, A., and Suga, S., 2003, "Development of Highly Loaded Fan With Tandem Cascade," AIAA Paper No. 2003–1065.
[13] Cumpsty, N. A., 2004, *Compressor Aerodynamics*, Kreiger, Malabar, FL.
[14] Smith, L. H., 1970, "Casing Boundary Layers in Multistage Axial-Flow Compressors," *Flow Research on Blading*, L. S. Dzung, ed., Elsevier, Amsterdam, pp. 275–304.
[15] Wellborn, S. R., and Okiishi, T. H., 1996, "Effects of Shrouded Stator Cavity Flows on Multistage Axial Compressor Aerodynamic Performance," NASA Report No. CR-198536.
[16] Wisler, D. C., 1977, "Core Compressor Stage Exit Study: Volume 1—Blade Design," NASA No. CR-135391.

Downloaded 28 May 2010 to 128.113.26.88. Redistribution subject to ASME license or copyright; see http://www.asme.org/terms/Terms_Use.cfm

[17] Wisler, D. C., 1987, "Secondary Flow, Turbulent Diffusion, and Mixing in Axial-Flow Compressors," ASME J. Turbomach., **109**, pp. 455–482.
[18] Swoboda, M., Ivey, P. C., Wenger, U., and Gummer, V., "An Experimental Examination of Cantilevered and Shrouded Stators in a Multistage Axial Compressor," ASME Paper No. 98-GT-282.
[19] Gallimore, S. J., Bolger, J. J., Cumpsty, N. A., Taylor, M. J., Wright, P. I., and Place, J. M. M., "The Use of Sweep and Dihedral in Multistage Axial Flow Compressor Blading Part 1: University Research and Methods Development," ASME Paper No. GT-2002-30328.
[20] Place, J. M. M., 1997, "Three-Dimensional Flow in Axial Compressors," Ph.D. thesis, University of Cambridge, Cambridge, UK.
[21] Place, J. M. M., Howard, M. A., and Cumpsty, N. A., 1996, "Simulating the Multistage Environment for Single Stage Compressor Experiments," ASME J. Turbomach., **118**, pp. 706–716.
[22] Camp, T. R., 1995, "Aspects of the Off-Design Performance of Axial Flow Compressors," Ph.D. thesis, University of Cambridge, Cambridge, UK.
[23] Howard, M. A., Ivey, P. C., Barton, J. P., and Young, K. F., 1994, "Endwall Effects at Two Tip Clearance in a Multistage Axial Flow Compressor With Controlled Diffusion Blading," ASME J. Turbomach., **116**, pp. 635–647.
[24] McGlumphy, J., 2008, "Numerical Investigation of Subsonic Axial-Flow Tandem Airfoils for a Core Compressor Rotor," Ph.D. thesis, Virginia Polytechnic Institute and State University, Blacksburge, VA.
[25] Lieblein, S., 1965, "Aerodynamic Design of Axial-Flow Compressors," Chap. 4, NASA Report No. SP-36.
[26] Hall, E. J., Heidegger, N. J., and Delaney, R. A., 1999, "ADPAC v1.0—User's Manual," NASA Report No. CR-1999-206600.

Downloaded 28 May 2010 to 128.113.26.88. Redistribution subject to ASME license or copyright; see http://www.asme.org/terms/Terms_Use.cfm